

Semimicroscopic algebraic description of α -clustering in ^{22}Ne

G. Lévai*

Institute for Nuclear Research, Hungarian Academy of Sciences (MTA Atomki),

H-4001 Debrecen, P.O. Box 51. Hungary

Abstract

The alpha-cluster states of ^{22}Ne are studied within the framework of the semimicroscopic algebraic cluster model (SACM). The band structure, energy spectrum as well as E2 and E1 transitions are calculated and are compared with the experimental data. The results are also compared with those obtained from two microscopic models: the deformed-basis antisymmetrized molecular dynamics (DAMD) approach and the generator-coordinate method (GCM). It is found that the prominent bands obtained in the latter frameworks all have equivalents in the SACM and the agreement between the calculated spectroscopic properties is rather good, especially for positive-parity states.

PACS numbers: 21.60.Gx, 21.60.Fw, 27.30.+t

*Electronic address: levai@atomki.mta.hu

I. INTRODUCTION

Clusterization is a special collective phenomenon that characterizes nuclei throughout the chart of nuclides. The most characteristic examples for clusterization have been found in light nuclei. These configurations show a variety both in the type of clusters (ranging individual nucleons to ^{12}C and ^{16}O) and their number (from two- to four-body systems and even beyond). The most typical cluster is the α particle, which is a tightly bound system of two protons and two neutrons. α cluster states are present in the low-lying spectrum of many light nuclei throughout the p and sd shell and typically appear as the members of well deformed collective bands.

In the theoretical description of clustering it is essential to include the relative motion of the clusters as the most important degree of freedom. However, since the cluster system as a whole consists of interacting fermions (nucleons), the effects of the Pauli exclusion principle also have to be taken into account. This can be done by using a basis in which the single-nucleon states appear in a fully antisymmetrized form. Such basis is used in *microscopic* cluster models [1], which also employ microscopic nucleon-nucleon interactions. *Phenomenological* cluster models follow a technically simpler approach in that their model space does not observe strictly the Pauli principle, and they employ effective cluster-cluster interactions. This is the case, for example, with some potential models [2]. *Semimicroscopic* cluster models typically combine a microscopic model space with effective interactions. Examples for this are the orthogonality condition model (OCM) [3] and the semimicroscopic algebraic cluster model (SACM) [4].

The SACM makes heavy use of the $\text{SU}(3)$ algebra, which appears in the description of both the relative motion and that of the internal cluster structure, where it accounts for the orbital sector in terms of Elliott's $\text{SU}(3)$ model [5, 6]. The $\text{SU}(3)$ algebra is the symmetry algebra of the three-dimensional harmonic oscillator and it is also used in the construction of the harmonic oscillator (or $\text{SU}(3)$) shell model. The connection between the shell and cluster approaches was established more than fifty years ago in the harmonic oscillator approximation [7] making use also of the $\text{SU}(3)$ formalism [8]. Based on this connection the model space of the SACM is a subset of the fully antisymmetrized $\text{SU}(3)$ shell model space, which also takes into account the assumed cluster configuration. It contains states with good $\text{SU}(3)$ symmetry, which are assigned to $\text{SU}(3)$ irreducible representations (irreps).

This symmetry-dictated truncation of the $SU(3)$ shell model space typically contains the most deformed states of the joint nucleus, reflecting the cluster configuration of the system, but less deformed states are also included usually. In fact, this method seems to be fairly effective in studying the shape isomers (e.g. superdeformed and hyperdeformed states) and the clusterizations associated with them [9].

It is notable that the $SU(3)$ symmetry seems to be a good approximation for many nuclei in the p and the sd shell apart from the cluster picture too. In Ref. [10] it was shown that an extremely simplified, essentially parameter-free Hamiltonian that contains only the harmonic term and the second-order Casimir operator of the $SU(3)$ algebra is able to account in this region for the trends of some basic observables (e.g. energy of the first excited opposite-parity level) of nuclei.

More recently much attention has been paid to nuclei in which a core system consisting of closed-shell clusters is surrounded by a few neutrons. In these systems the neutrons can be pictured as moving on molecular orbitals around the core configuration. Typical examples are the Be isotopes, in which the neutrons surround two α particles [11]. Neon isotopes have been proposed as the next possible examples, in which the neutrons orbit around the $^{16}\text{O} + \alpha$ core [12]. These systems can also be described in the antisymmetrized molecular dynamics (AMD) approach [13] or its extension, the deformed-basis AMD (DAMD) [14]. This microscopic approach does not assume a cluster structure from the beginning and can describe systems in which both the shell and cluster structures, or their mixture play a role.

Here we discuss the ^{22}Ne nucleus in terms of the semimicroscopic algebraic cluster model. Our aim is not only the theoretical interpretation of the experimental spectroscopic information (band structure, spectrum, electromagnetic transitions) but also comparing the performance of the SACM with that of microscopic approaches, the GCM [15, 16] and the DAMD [17]. The SACM shares some common features with these models and it is worthwhile to investigate whether these manifest themselves in the results. The GCM employs a microscopic model space constructed from harmonic oscillator orbitals such that the oscillator parameter is common for each cluster. This technical assumption is also used in defining the model space of the SACM. Furthermore, both models consider excited states of the core cluster. In the SACM these states are those belonging to the ground-state $SU(3)$ configuration of the core, while in the GCM they can be selected independently. The common feature of the SACM and the DAMD is the ability of these models to give a joint

description of shell-like and cluster-like configurations in the same system. In the SACM this is again due to the $SU(3)$ basis, which is a subset of the $SU(3)$ shell model basis. As such, it contains states with well developed cluster structure typically appearing around the threshold energy of the assumed cluster configuration, but also shell model-like states in or around the ground-state region.

The paper is structured as follows. In Sec. II we present the main features of the SACM. Section III contains the SACM description of the ^{22}Ne nucleus in terms of the $^{18}\text{O}+\alpha$ configuration, while in Sec. IV the results are compared with those obtained from the GCM and DAMD approaches. Finally, conclusions are drawn in Sec. V.

II. THE SEMIMICROSCOPIC ALGEBRAIC CLUSTER MODEL

Here we review the basics of the SACM [4] for the core+ α states of even-even nuclei. This model has been applied previously to a number of core+ α systems [18, 19]. It was shown that the parameters fitted to the spectrum of nuclei in the $A = 16$ to 20 domain vary in a consistent way [20]. This correlated behavior was interpreted for $A = 18$ to 20 nuclei in terms of a new cluster supersymmetry scheme [21], in which the bosonic degree of freedom was associated to the excitations of the relative motion, while the fermionic structure was represented by 0, 1 or 2 holes in the p shell. Other cluster structures with heavier clusters were also discussed in terms of the SACM [22].

A. The model space

The relative motion (indexed by ‘ R ’) is described by the group structure

$$\begin{array}{ccccccc} U_R(4) & \supset & SU_R(3) & \supset & SO_R(3) & \supset & SO_R(2) \\ [N, 0, 0, 0] & & (n_\pi, 0) & & L_R & & M_R, \end{array} \quad (1)$$

where $n_\pi = N, N-1, \dots, 1, 0$, $L_R = n_\pi, n_\pi-2, \dots, 1$ or 0 , $M_R = L_R, L_R-1, \dots, -L_R$. Here $N = n_\pi + n_\sigma$ is the total number of bosons, n_π is the number of dipole bosons, i.e. oscillator quanta assigned to the relative motion of the clusters, while n_σ is the number of scalar bosons. The role of these latter bosons is essentially introducing an upper cut-off in the model space, making it finite. There is also a lower cut-off in the number of dipole

bosons due to the Wildermuth condition, which is necessary to take into account the Pauli principle. This minimal number of n_π is determined by the structure of the two clusters. In core+ α systems it is determined by the core nucleus. For cores taken from the sd shell it is usually $n_{\pi \text{ min}} = 8$ corresponding to lifting the four nucleons of the α particle to the $2\hbar\omega$ shell from the $0\hbar\omega$ shell. The parity assigned to the relative motion is $(-1)^{n_\pi}$.

It is important to note that the procedure that determines the model space by matching the SU(3) cluster model space with the SU(3) shell model space eliminates the Pauli-forbidden states, so it also enforces the Wildermuth condition.

The core nucleus is described in terms of Elliott's SU(3) shell model [5, 6]. This model assigns an $SU_C(3)$ representation to the orbital structure of the core nucleus (hence the index C), while the spin-isospin structure is described by Wigner's SU(4) supermultiplet scheme that handles the spin and isospin structure in a combined way. The orbital and isospin structures are interrelated by the antisymmetry requirement. In practice this means that in the maximally symmetric orbital structure that characterizes the ground-state configuration of the core nucleus comes together with maximally antisymmetric spin-isospin structure, which, in general, prescribes low values of S and T . For even-even nuclei this implies $S = 0$ and $T = (N - Z)/2$. This is the case for the α particle too, with $S = 0$ and $T = 0$. In this case, furthermore, the ground-state orbital structure is described by the scalar (0,0) SU(3) representation with $L = 0$ orbital angular momentum. In practice this means that the internal structure of the α particle does not have direct influence on the construction of the model space.

It is worth mentioning that it is possible to consider in the core sector configurations that correspond to excited states either with $0\hbar\omega$ or even $1\hbar\omega$. However, this is not typical and has not been applied up to now.

The orbital part of the core+ α system is determined by the SU(3) coupling of the representations assigned to the relative motion and the core nucleus. In the general case this is done as

$$\begin{array}{ccccccc} SU_C(3) \otimes SU_R(3) & \supset & SU(3) & \supset & SO(3) & \supset & SO(2) \\ (\lambda_C, \mu_C) \quad (n_\pi, 0) & & (\lambda, \mu) & & \kappa L & & M \end{array} . \quad (2)$$

The (λ, μ) SU(3) irreps in (2) are obtained from the direct product

$$(\lambda_C, \mu_C) \times (n_\pi, 0) = \sum_{\lambda\mu} m_{\lambda\mu} (\lambda, \mu) \quad , \quad (3)$$

with multiplicity $m_{\lambda\mu}$. When one of the SU(3) representations has either $\lambda = 0$ or $\mu = 0$ (as is the case for any core+ α system), each resulting representation has multiplicity one.

The cluster model space constructed in this way contains states (SU(3) representations) that are not allowed by the Pauli principle. The final model space is obtained after matching the set of SU(3) states from Eq. (3) with the fully antisymmetrized SU(3) shell model space. This procedure also eliminates the spurious center of mass excitations.

The (λ, μ) SU(3) representations determine the SO(3) representations contained in them, i.e. the orbital angular momenta L . Here the κ quantum number also plays an important role in resolving the multiplicities of the L quantum numbers contained in the same SU(3) representation. The general rule is

$$\begin{aligned} \kappa &= \min[\lambda, \mu], \min[\lambda, \mu] - 2, \dots 1 \text{ or } 0; \\ L &= \kappa, \kappa + 1 \dots \kappa + \max[\lambda, \mu] \text{ for } \kappa \neq 0 \text{ and} \\ L &= \max[\lambda, \mu], \max[\lambda, \mu] - 2, \dots 1 \text{ or } 0 \text{ for } \kappa = 0. \end{aligned} \quad (4)$$

In practice κ identifies complete bands for even-even nuclei as, in general, it plays the role of K , the projection of the angular momentum on the symmetry axis of the nucleus. This means that each SU(3) representation contains one or more complete rotational bands in this case. Breaking this result down to the various SU(3) representations one finds that representations of the type $(\lambda, 0)$ and $(\lambda, 1)$ contain a single rotational band with $\kappa = 0$ and 1, respectively. Representations of the type $(\lambda, 2)$ contain two bands with $\kappa = 0$ and 2, $(\lambda, 3)$ also contain two bands with $\kappa = 1$ and 3, while $(\lambda, 4)$ contains three, with $\kappa = 0, 2$ and 4.

The SU(3) representations are also indicative about the deformation of the joint nucleus, because in the SU(3) scheme these quantum numbers are related to the difference of the distribution of oscillator quanta in the three directions. Accepting the usual notation and assuming that these numbers are related by $n_z \geq n_x \geq n_y$, the λ and μ quantum numbers are expressed as $\lambda = n_z - n_x$ and $\mu = n_x - n_y$. This means that $\mu = 0$ corresponds to a prolate deformation, while $\lambda = 0$ to an oblate deformation. When neither λ and μ are zero, then the nucleus is triaxial. Nevertheless, small μ and large λ describes a near prolate structure [6].

The parity of the α -cluster states is determined by n_π , because the parity assigned to the core configuration is uniquely defined, as is the parity of the α particle. The general form of the SACM basis for an even-even core+ α configuration is written as

$$|Nn_\pi, (\lambda_C, \mu_C); (\lambda, \mu)\kappa LT\rangle . \quad (5)$$

As it was discussed above, this basis is fully microscopic by construction. Note that the short-hand notation $n_\pi(\lambda, \mu)\kappa$ can be used to identify the individual bands whenever only a single core configuration is taken into account.

B. The Hamiltonian

The phenomenological SACM Hamiltonian is expressed in terms of boson number conserving combinations of the group generators. In the simplest applications it is sufficient to consider terms up to second order [4]. A further assumption is considering only terms constructed from the Casimir invariants of the corresponding groups. This is called the dynamical symmetry approximation. In the case of SU(3) dynamical symmetry one typically considers a Hamiltonian of the type

$$\begin{aligned} H = & \hbar\omega C_1(\text{U}(3)) + \chi_R C_2(\text{SU}_R(3)) + \chi C_2(\text{SU}(3)) \\ & + \theta K^2 + \beta C_2(\text{SO}(3)) + E_0 . \end{aligned} \quad (6)$$

Here the first term is an harmonic oscillator with the parameter $\hbar\omega$ determined in MeV by the mass number as $\hbar\omega = 45A^{-1/3} - 25A^{-2/3}$ for light nuclei, while E_0 is a constant that sets the ground-state energy to zero. The $C_2(\text{SU}(3))$ Casimir operators correspond to the combinations of the respective quadrupole-quadrupole and squared angular momentum terms. $C_2(\text{SO}(3))$ is the Casimir operator of the SO(3) group and it is equivalent with the square of the angular momentum operator. The K^2 operator is used to generate K -band splitting in the Elliott model, i.e. to lift the degeneracy of states with the same L and different κ values [24]. It can be defined as the square of the L_3 component of the angular momentum, which is the projection of L on the body-fixed symmetry axis of the nucleus. It can be written as a special combination of three rotational scalar interactions constructed from the L angular and Q quadrupole moment operators [24]. It was also shown that it is close to being diagonal in the Elliott basis, so it is customary to neglect

its off-diagonal terms. This term splits the energy of states with the same SU(3) labels and angular momenta. Taking the SU(3) basis (5) with the assumptions mentioned above the Hamiltonian (6) is diagonal, and the eigenvalues are given by

$$E = \hbar\omega n_\pi + \chi_R n_\pi (n_\pi + 3) + \chi(\lambda^2 + \mu^2 + \lambda\mu + 3\lambda + 3\mu) + \theta\kappa^2 + \beta L(L + 1) + E_0 . \quad (7)$$

It is notable that the eigenvalues of $C_2(\text{SU}(3))$ are largest for the leading SU(3) representation that corresponds to maximal deformation. Due to the nature of the nuclear forces such states are always located at low energy compared to other representations from the same shell (same n_π). Since these states always appear in the SACM basis, it means that clustering implies the presence of maximally deformed states in the SU(3) basis.

The θ parameter of the κ^2 term is often considered to be dependent on n_π , or at least on $(-1)^{n_\pi}$ on grounds that bands with $K = 2$ typically occur above $K = 0$ bands for positive-parity levels, while for the negative-parity spectrum states with $J^\pi = 3^-$ or 2^- appear lowest, indicating that bands with $K = 3$ or 2 should lie below bands with $K = 1$ and 0 , respectively. Since such low-lying negative-parity bands typically appear in *sd*-shell nuclei, in previous applications of the SACM in this domain this situation was handled on the phenomenological level by considering n_π -, or parity-dependent κ^2 terms [19, 22]. It is also possible to take into account the different moments of inertia associated to different bands. For this one can consider $\beta = \beta_0 / \langle C_2(\text{SU}(3)) + 3 \rangle$, because the SU(3) Casimir operator also expresses the measure of the deformation.

C. Electromagnetic transitions

Here we discuss only E2 and E1 transitions. The E2 transitions are generated by quadrupole operators assigned both to the relative motion and the internal structure of the clusters (in this case this means the core), which are rank-2 tensors in terms of the SO(3) rotational group. These operators are also SU(3) tensors with SU(3) character (1,1) and angular momentum 2. The electric quadrupole transitions containing one-body terms are thus generated by the two-parameter operator

$$T^{(\text{E2})} = q_R Q_R^{(1,1)2} + q_C Q_C^{(1,1)2} . \quad (8)$$

The selection rules of this operator are as follows. It allows only intrashell transitions, i.e. n_π is conserved. Besides in-band transitions it allows changing κ by 2 units and leaving λ and μ unchanged. Transitions with $\Delta\lambda = \pm 2$ and $\Delta\mu = \mp 1$ are also allowed, although they are typically much weaker than in-band transitions. When $q_R = q_C$ the operator corresponds to the quadrupole momentum of the joint $SU(3)$ group. In this case (8) generates transitions only within the same $SU(3)$ representations, so only κ can change.

In order to describe transitions between major shells with $\Delta n_\pi = \pm 2$ it is necessary to add two-body terms to (8) acting only on the relative motion part of the states. (The excitations of the core nucleus are restricted to states belonging to the ground-state $SU_C(3)$ representation, so excited-shell core states are missing from the model space.) This operator can be constructed as

$$T_{\text{intershell}}^{(E2)} = p_R \left\{ [[\sigma^\dagger \times \tilde{\pi}]^{(0,1)} \times [\sigma^\dagger \times \tilde{\pi}]^{(0,1)}]^{(0,2)2} + [[\tilde{\sigma} \times \pi^\dagger]^{(1,0)} \times [\tilde{\sigma} \times \pi^\dagger]^{(1,0)}]^{(2,0)2} \right\} \quad (9)$$

and its $SU_R(3)$ character is $(\lambda_R, \mu_R) = (0, 2)$ for transitions with $\Delta n_\pi = -2$ and $(\lambda_R, \mu_R) = (2, 0)$ for transitions with $\Delta n_\pi = 2$. The selection rules for the two processes are given by the appropriate $SU(3)$ multiplication rule [4], i.e. strong transitions are expected for $\Delta n_\pi = \pm 2$, $\Delta\lambda = \pm 2$, $\Delta\mu = 0$, while weaker transitions with $\Delta n_\pi = \pm 2$, $\Delta\lambda = 0$, $\Delta\mu = \pm 1$.

The electric dipole operator connects shells with $\Delta n_\pi = \pm 1$. It is not an $SU(3)$ tensor, rather it has mixed $SU(3)$ character of $(\lambda, \mu) = (1, 0)$ and $(0, 1)$:

$$T^{(E1)} = d_R [[\sigma^\dagger \times \tilde{\pi}]^{(0,1)} + [\tilde{\sigma} \times \pi^\dagger]^{(1,0)}] \quad . \quad (10)$$

For $\Delta n_\pi = \mp 1$ it generates strong transitions with $\Delta\lambda = \mp 1$ and $\Delta\mu = 0$ and weaker transitions with $\Delta\lambda = \pm 1$ and $\Delta\mu = \mp 1$ [4].

The transition matrix elements composed of the transition operators (e.g. (8)) and the basis states (5) can be calculated using $SU(3)$ and $SO(3)$ tensor algebraic manipulations that include $SO(3)$ $6j$ coefficients, $SU(3)$ $9j$ coefficients, $SU(3)$ isoscalar factors and reduced matrix elements. See e.g. Ref. [21] for the details.

III. APPLICATION TO ^{22}Ne

In our approach we assume that the Hamiltonian has dynamical symmetry, so the energy eigenvalues can be calculated exactly. This also means that the spectrum contains rotational

TABLE I: SU(3) representations contained in the SACM model space of $^{22}\text{Ne} \sim \alpha + ^{18}\text{O}$ up to $4\hbar\omega$ excitations (i.e. up to $n_\pi = 12$).

n_π	(λ, μ)
8	(8,2) (6,3) (4,4)
9	(11,1) (9,2) (7,3) (5,4)
10	(14,0) (12,1) (10,2) (8,3) (6,4)
11	(15,0) (13,1) (11,2) (9,3) (7,4)
12	(16,0) (14,1) (12,2) (10,3) (8,4)

bands with energy dependence of the type $E \sim J(J+1)$. Obviously, this is not the case in general: typically only the most characteristic cluster bands (with $K=0$) show clear rotational pattern in the experimental energy spectrum. In a more realistic calculation, when the Hamiltonian is not diagonal one would expect such a result. The application of the SACM with broken SU(3) dynamical symmetry can be found in Ref. [23]. The deviation from the rotational pattern would be more pronounced for bands that contain unnatural-parity states, because the composition of these states from various SU(3) representations would be different from that of natural-parity states. This is because unnatural-parity states appear only in basis states with $\mu \neq 0$, while natural-parity states appear in any (λ, μ) representation.

The core nucleus for ^{22}Ne is ^{18}O . In the Elliott scheme its ground-state configuration is described by the (4,0) $\text{SU}_C(3)$ representation that contains the 0^+ ground state and the first excited $2^+(1.98)$ and $4^+(3.55)$ states. The spin-isospin structure is $T=1$ and $S=0$, which means that the orbital angular momentum is responsible for the J angular momentum of the nucleus. The model space for ^{22}Ne is displayed in Table I.

A. The band structure

The ground-state region should be dominated by configurations with $n_\pi = 8$, i.e. $0\hbar\omega$ excitations. Of these the dominant one is expected to lie lowest in energy, which is the (8,2) representation. This contains two bands with $\kappa = 0$ and 2, of which the latter one is expected to lie higher, similarly to other neighboring nuclei (e.g. ^{24}Mg). The next positive-parity band in energy could be from the (6,3) SU(3) representation, which may have a lower-lying $\kappa = 1$ and a higher-lying $\kappa = 3$ band. We note here that in the Elliott model the model space of ^{22}Ne with the appropriate permutational structure contains 13 SU(3) representations for $0\hbar\omega$ i.e. $n_\pi = 8$, some with multiplicities [6]. The SACM model space contains only three of them (see Table I), including the two leading ones, (8,2) and (6,3) with the largest deformation, which are expected to be located lowest in excitation energy.

The low-lying negative-parity spectrum should contain states from the leading (11,1) representation, which corresponds to nearly prolate deformation and has a single band with $\kappa = 1$. States from the (9,2) with $\kappa = 0$ and 2 should also lie close. The deformation of these states is similar to that of the (8,2) configuration in the ground-state region. The difference is that in contrast with the positive-parity spectrum, here the $\kappa = 2$ band is expected to be below the $\kappa = 0$ band.

Somewhat higher the $2\hbar\omega$ states should appear with $n_\pi = 10$. The leading SU(3) representation here is (14,0), which corresponds to a highly deformed prolate structure with states forming a $\kappa = 0$ rotational band. Further up in energy the states from the (12,1) representation with $\kappa = 1$ are also expected to appear. This configuration is also close to a highly deformed prolate shape.

The negative-parity correspondent of the (14,0) band is (15,0), which is also a highly deformed configuration composed of states belonging to a $\kappa = 0$ band.

Further positive-parity $\kappa = 0$ bands may appear in or above this region with $n_\pi = 8$ $(\lambda, \mu) = (4, 4)$ or $n_\pi = 10$ $(\lambda, \mu) = (10, 2)$, depending on the parameters of H . The former one would be a compact, triaxial structure, while the latter one would correspond to a close to prolate shape with relatively large deformation.

In assigning the experimental states to bands one can use the relative position of the energy levels (e.g. rotation structures) and electromagnetic transition data. We combine these with the band assignment of other works [15, 17], making an effort to assign all the

low-lying experimental states to model ones for every J^π . The band structure we apply in the case of ^{22}Ne is displayed in Tables II and III for positive- and negative-parity states, respectively. We used experimental data taken from the Brookhaven National Laboratory data base [25].

B. The energy spectrum

We apply (7) to fit the energy eigenvalues. The oscillator constant for $A = 22$ is $\hbar\omega = 12.88$ MeV according to the formula cited after Eq. (6). If the anharmonic $C_2(\text{SU}_R(3))$ term associated to the relative motion is neglected by setting $\chi_R = 0$, the band-head energies can be estimated from the graph displayed in Figure 1, where the location of various $\text{SU}(3)$ states is plotted as the function of parameter χ . The actual band-head energies are also influenced by the $\theta\kappa^2$ term for bands with $\kappa \neq 0$, and to a small extent also by the rotational term $\beta L(L+1)$ when $L \neq 0$ holds for the band-head state, nevertheless, Fig. 1 gives reasonable support to estimate the sequence of bands.

The assignment of experimental levels to model states is contained in Tables II and III for positive- and negative-parity states, respectively.

The β parameter sets the steepness of the rotational bands. Since this depends on the moment of inertia, which, in turn depends on the deformation, we parametrized it as $\beta = \beta_0/(\lambda^2 + \mu^2 + \lambda\mu + 3\lambda + 3\mu + 3)$, taking into account the eigenvalues of the $C_2(\text{SU}(3))$ operator for each band.

The κ^2 term seems to exhibit parity dependence, as the 2^+ band appears above the ground-state 0_1^+ band, while for the negative-parity levels the 2^- band is the lowest. For this reason we consider different values of θ for positive- (θ_+) and negative-parity (θ_-) bands. Similarly to the rotational constant β we also parametrized the κ -dependent terms with the factor $(\lambda^2 + \mu^2 + \lambda\mu + 3\lambda + 3\mu + 3)^{-1}$ reflecting the effect of deformation.

In conclusion, there are four parameters that should be determined from the fit to the experimental data: χ , θ_+ , θ_- and β_0 . Of these the first three determine the location of the band heads (although β_0 also has a slight influence on bands with $\kappa \neq 0$). Since in the fit we wished to consider also bands belonging to $3\hbar\omega$ and $4\hbar\omega$ excitations ($n_\pi = 3$ and 4), we also included the anharmonic term associated with the relative motion. Allowing $\chi_R \neq 0$ in

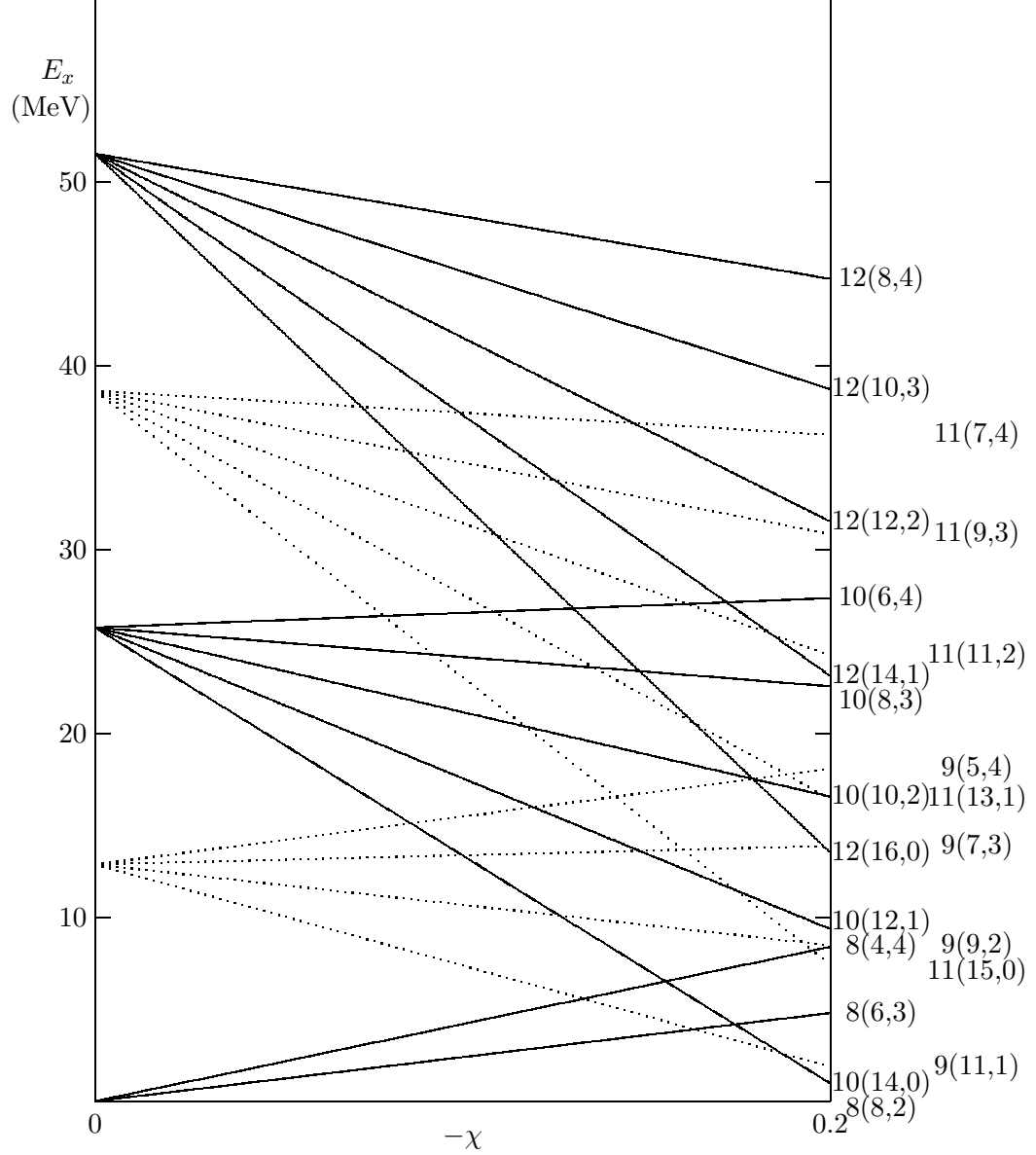


FIG. 1: Estimation of the band-head energies as the function of the χ parameter with even (full line) and odd (dotted line) parity. To the right the quantum numbers $n_\pi(\lambda, \mu)$ are displayed in separate columns for even- and odd-parity bands. Bands with $n_\pi \leq 12$ are displayed. The lowest band with $n_\pi = 13$ would appear at $E_x = 19.2$ MeV for $\chi = -0.2$.

Eq. (7) modifies the relative position of bands with different n_π , but has no direct influence on the relative position of bands (SU(3) multiplets) with the same n_π .

The fitted parameters (in MeV) are $\chi_R = -0.1027$, $\chi = -0.1227$, $\theta_+ = 101.929$, $\theta_- = -57.713$ and $\beta_0 = 18.862$. The calculated energy eigenvalues are displayed in Tables II and III along with the corresponding experimental energy values and the relevant K^π band labels. These latter ones include labels generally accepted in the experimental assignment

of levels, but also some assignments from theoretical works [15, 17]. The assignment of individual levels to bands in these works occasionally differs from our choice. The positive- and negative-parity energy spectrum is also displayed in a rotational diagram form in Figs. 2 and 3, respectively. Note that the figures contain only model bands that correspond to well-established experimental bands, or can be candidates for bands predicted by other models [15, 17].

It is seen that the calculated positive-parity band structure reproduces the experimental levels rather well. The $8(8,2)2$ and $8(6,3)1$ bands have rotational structure in the calculations, while their experimental counterparts have even-odd staggering character. As we have mentioned earlier, such a feature could be reproduced in calculations with a Hamiltonian that does not have exact dynamical symmetry, and the energy eigenvalues would be calculated by diagonalization. Then the natural- and unnatural-parity states would have different composition that may lead to an even-odd staggering pattern.

The band-head energy of the calculated negative-parity bands is somewhat different from those of the experimental ones. The calculations predict the $9(11,1)1$ band lowest around $E_x = 4$ MeV, about 3 MeV's lower than the experimental counterpart at 7.051 MeV. In contrast, the $9(9,2)2$ and $9(9,2)0$ bands lie about 2 MeV too high. It seems that the simple Hamiltonian (6) is not flexible enough to reproduce all the details of the band structure. The κ -dependent term in the negative-parity spectrum may also be too simple to get all the bands at the correct position.

It is notable that bands corresponding to highly deformed prolate structure appear in the energy domain where molecular bands are expected to appear, i.e. around 12 to 18 MeV. These include the positive-parity $(12,1)1$ and $(10,2)0$ bands with $n_\pi = 10$, the $(16,0)0$ band with $n_\pi = 12$ and the negative-parity bands $(15,0)0$ and $(13,1)1$ with $n_\pi = 11$ (see Tables II and III).

C. E2 transitions

The experimental data contain only $B(E2)$ values for transitions corresponding in the SACM to $\Delta n_\pi = 0$, $\Delta \lambda = 0$, $\Delta \mu = 0$, so we apply the operator (8) with $q_R = q_C$. Tables IV and V show the transitions calculated in this approximation. The $q_R = q_C$ parameter was fitted to the transition with the lowest known experimental error [25] and it was found to be

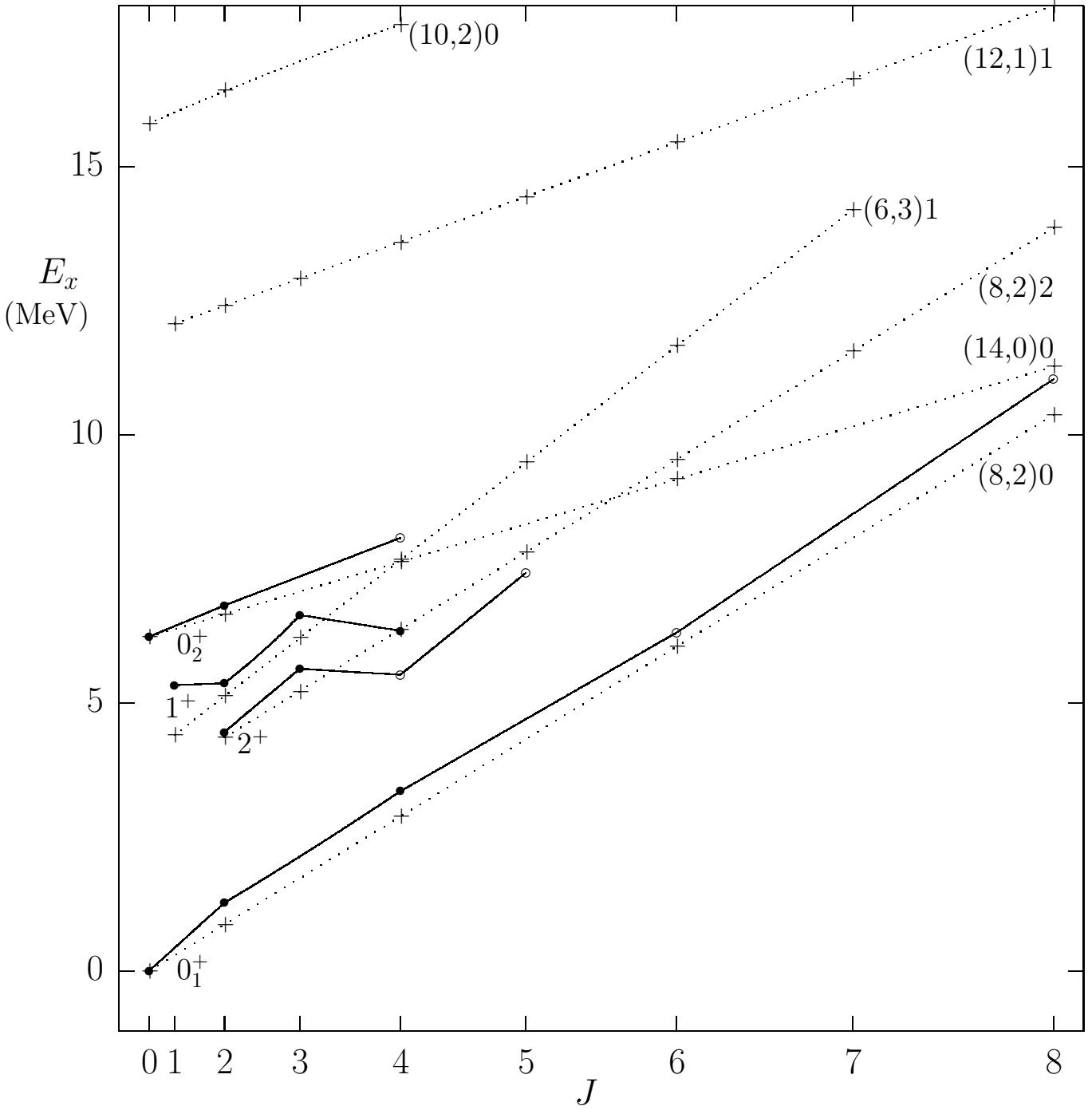


FIG. 2: Positive-parity bands displayed in a rotational diagram form. Experimental bands are indicated with full line and K^π , while those predicted by the SACM are marked with dotted line and the $(\lambda, \mu)\kappa$ labels. Open circles denote experimental states with uncertain J^π assignment.

$1.11 \text{ (W.u.)}^{1/2}$, which corresponds to 1.914 e fm^2 for ^{22}Ne . We also displayed the calculated results from Refs. [17] and [15]. We note that the experimental data we used [25] differ somewhat from those displayed these latter works.

The calculated values are in good agreement with the altogether six experimental data,

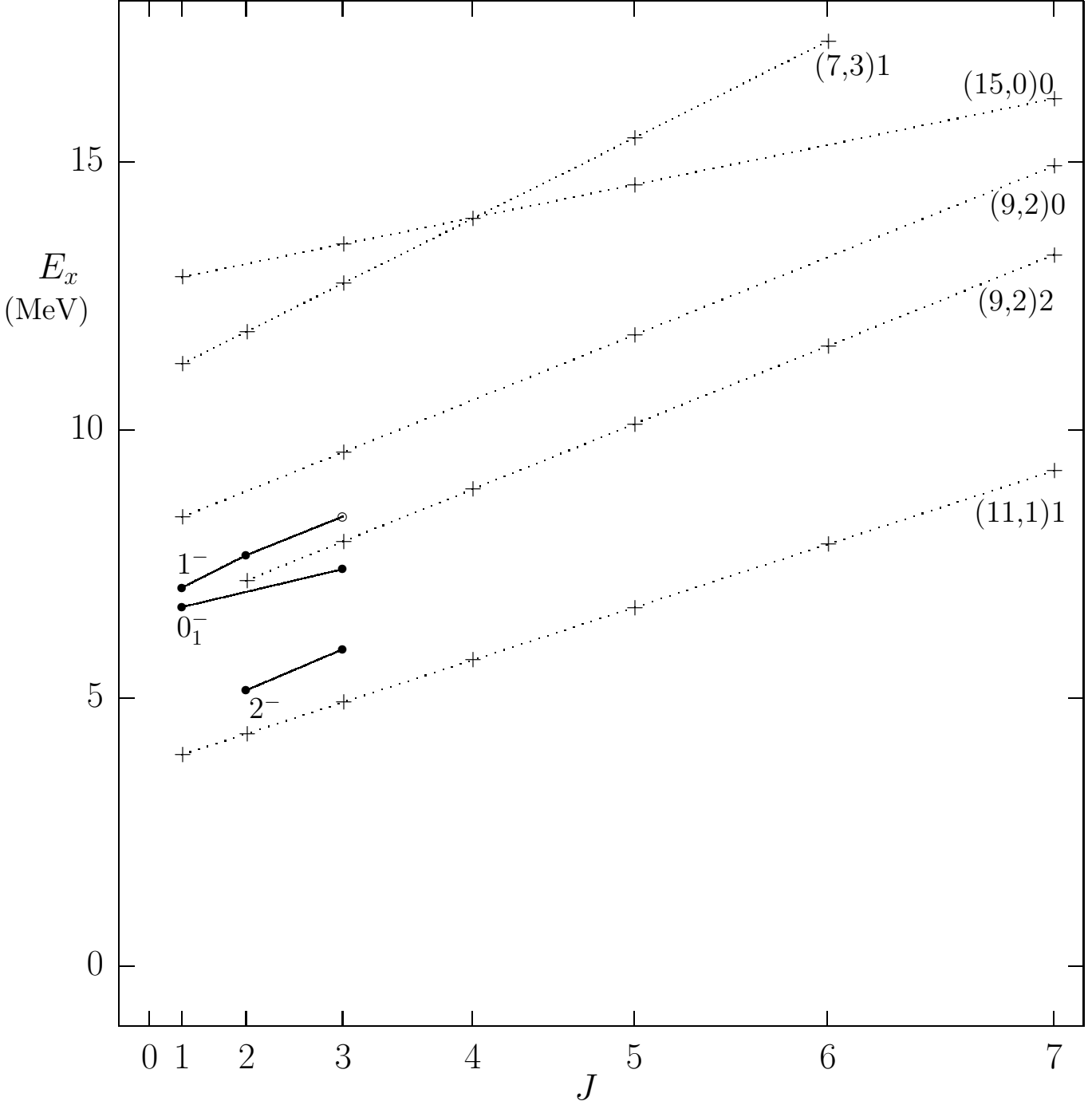


FIG. 3: The same as Fig. 2 for negative-parity bands.

two of which are lower limits and concern in-band transitions in the 0_1^+ and 2^+ bands. Note that there are no experimental data for transitions between negative-parity levels.

The fitted parameter was also used to calculate the electric quadrupole moment of the 2_1^+ state. It was found to be -22.984 e fm^2 , which is just within the error bar of the experimental value of $-19 \pm 4 \text{ e fm}^2$ [26].

For $q_R \neq q_C$ the selection rule concerning (λ, μ) is relaxed somewhat and transitions

described in Subsection II C become allowed.

D. E1 transitions

There is a single known experimental $B(E1)$ value in the compilation Ref. [25], and we used this to fit the d_R parameter appearing in Eq. (10). The results are displayed in Table VI. The SACM predicts relatively strong E1 transitions from the 0_1^- band to the 0_1^+ ground-state band and from the 2^- band to the 2^+ band. Transitions from the 2^- band to the 0_1^+ band are significantly weaker, i.e. they are of the order 10^{-7} to 10^{-6} W.u., while transitions from the 0_1^- to the 2^+ band are forbidden. There are also transitions to the 0_1^+ and 2^+ bands from the bands assigned to the $(\lambda, \mu) = (7, 3)$ SU(3) quantum numbers, but these are about an order of magnitude weaker than those from the bands labelled with (9,2).

IV. COMPARISON WITH THE RESULTS OF MICROSCOPIC CLUSTER APPROACHES

Here we compare our results with those presented in Refs. [17] and [15, 16]. The former work [17] employs the deformed-basis antisymmetrized molecular dynamics (DAMD) method and describes the ^{22}Ne nucleus as a $\alpha + ^{16}\text{O}$ core surrounded by two neutrons occupying molecular orbitals. In this study there are five different energy surfaces that give rise to six bands (0_1^+ , 2^+ , 0_2^+ , 2^- , 1^- and 0_1^-) for which experimental counterparts can be identified in the spectrum of ^{22}Ne . The internal structure of these bands has been described in Ref. [17], and it was found that the 1^- , 0_2^+ and 0_1^- bands are based on a well-developed $\alpha + ^{16}\text{O}$ structure, while the 0_1^+ , 2^+ and 2^- bands correspond to a more compact structure. Besides these bands $\alpha + ^{18}\text{O}_{\text{g.s.}}$ type molecular bands are also discussed in Ref. [17] by extending the calculations to a hybrid-GCM approach. This extension led to two more bands denoted by 0_3^+ and 0_2^- starting near $E_x = 15$ MeV.

The other approach [15] makes use of the generator-coordinate method (GCM) and describes the ^{22}Ne nucleus as a ^{16}O core surrounded by an α particle and a dineutron. This method takes into consideration the 0^+ ground state and the first excited 2^+ state of the ^{18}O nucleus. The internal cluster wavefunctions are constructed in terms of the harmonic oscillator model with a common oscillator parameter, and the total wavefunction is fully

antisymmetrized. This method gives rise to several bands both with positive and negative parity, furthermore, it also describes nuclear molecular type bands near the $\alpha + {}^{18}\text{O}$ threshold. Later the GCM was also applied in the extended two-cluster model (ETCM), in which fourteen different internal ${}^{18}\text{O}$ states were considered with positive parity and $J \leq 4$ [16].

Here we compare the band structure and the spectroscopic properties of α -cluster structures in ${}^{22}\text{Ne}$ obtained from the DAMD, GCM and SACM approaches. We consider separately positive- and negative-parity bands at low energy, as well as nuclear molecular bands near the $\alpha + {}^{18}\text{O}$ threshold.

A. Low-lying positive-parity bands

The members of the 0_1^+ ground-state band are well-established experimentally up to $J^\pi = 8^+$ and are reproduced in all the models. In the SACM this band belongs to the (8,2) SU(3) configuration, which correspond to an elongated triaxial structure. The DAMD results [17] also indicate a similar structure, although the $\alpha + {}^{16}\text{O}$ configuration does not appear in the density plots. This is not a contradiction with the SACM results, because the model space of this latter model also includes shell-model-like states (SU(3) multiplets) that also appear in the cluster model space. The intensities of the in-band electric quadrupole transitions are also close in the DAMD and in the SACM, and both are rather close to the experimental values, as it can be seen from Table IV. However, the GCM [15] results (and the comparable ETCM ones [16]) are weaker by a factor of about 0.6.

There is some ambiguity in the assignment of experimental states to the $K^\pi = 2^+$ band [15, 17]. Due to the lack of $B(\text{E}2)$ data the identification of the band members is mainly based on their expected energy. The DAMD and SACM reproduce the band-head energy reasonably well, while in the GCM it comes out about 2 MeV too low. In all three models this band follows a regular rotational pattern, while the experimental energies show some odd-even staggering, depending on the assignment of states. Comparing the electric quadrupole transition intensities one finds that the DAMD and the GCM (as well as the ETCM) give comparable results, while the SACM values are somewhat larger. Transitions from this band to the 0_1^+ ground-state band were calculated in the GCM and the SACM, and they are in general agreement both with the few experimental data and with each other.

The 1^+ band is seen in the GCM and the SACM, but not in the DAMD. This may be due

to the relatively small deformation that may not lead to an easily identifiable energy surface in the latter model. The assignment of the lowest two states of this band is the same in both models, but there is a difference in the assignment of the states with higher J . Both models predict the band-head energy somewhat low, and both models fail to reproduce the odd-even staggering effect. There are no known $B(E2)$ values from experiment, and calculations are available only in the SACM: the typical intensity of transitions is somewhat weaker than those within the 2^+ band.

The 0_2^+ band appears in all three models, although its band head comes out 2 MeV too low in the GCM. In the SACM this band corresponds to an elongated prolate structure with $2\hbar\omega$ excitation, while in the DAMD it corresponds to a well-developed $\alpha + {}^{16}\text{O}$ cluster structure and two neutrons occupying a pf orbit around it. This interpretation is rather similar to the SACM description. Furthermore, the $B(E2)$ values are also rather close in the two models, while the GCM results fall behind them by about a factor of 5. It is notable that these latter values are close to those calculated for the $(4,4)0$ band in the SACM, which is expected in this region (see Table II) and has no correspondent in the other models. $E2$ transition from the 0_2^+ band to the 0_1^+ ground-state band are rather weak in the GCM ($B(E2) \leq 0.042$ W.u. [15]), and this is in accordance with the SACM prediction, according to which these transitions are forbidden in the $SU(3)$ dynamical symmetry limit.

Before closing this subsection it is worthwhile to compare the SACM, DAMD and GCM results with those obtained from the shell model [27]. In this latter work the $(sd)^6$ configuration is discussed, assuming an inert ${}^{16}\text{O}$ core structure. The $T = 1$ model space of this calculation must contain the equivalents of the $0\hbar\omega$ states of the SACM, i.e. the states with largest deformation and lowest excitation energy. Several bands are identified in Ref. [27], including 0_1^+ and 2^+ seen in all three models discussed here. A 4^+ band is also proposed built on the second 4^+ state located at 5.52 MeV. Neither other models discussed here expect a 4^+ band at such low energy, rather this state (with tentative $J = 4$ assignment) can be interpreted as the member of the 2^+ band, which exhibits a staggering pattern, and this may explain the relatively low energy of its 4^+ member. A 1^+ and a 3^+ state also appear close to the experimental states at 5.332 MeV and 6.635 MeV, although they are not mentioned explicitly as a possible band. Nevertheless, a 1^+ band is expected in this energy range both in the SACM and the GCM. The electric quadrupole transition intensities calculated in Ref. [27] are in reasonable agreement with those obtained from the other models. In particular,

transition intensities within the 0_1^+ band are rather close to the SACM and DAMD results, while $K^\pi = 2^+ \rightarrow 0_1^+$ transitions agree well with the findings of the SACM and GCM. Transitions within the 2^+ band are generally weaker than those predicted by either of the three models, but are close to the range of the DAMD and GCM results. In summary, the shell model results on the low-lying positive-parity states [27] are generally consistent with those obtained from the SACM, DAMD and GCM calculations. On the one hand this is not surprising considering the shell model background of some of these models, while on the other hand it is remarkable that some predictions of calculations done 40 years ago were verified by more accurate experiments performed since then.

B. Low-lying negative-parity bands

The lowest-lying negative-parity experimental band is $K^\pi = 2^-$. In terms of the DAMD this is interpreted as a proton excited core structure with nucleon density not showing pronounced α clustering. In the SACM this band can be interpreted as the $(\lambda, \mu)\kappa = (9, 2)2$ state with $1\hbar\omega$ excitation. It is notable that the nucleon density characterizing this band in the DAMD is rather similar to that of the 0_1^+ and 2^+ bands [17]. This is in line with the interpretation within the SACM: the (8,2) and (9,2) SU(3) states have rather similar deformation. A 2^- band is also described by the GCM [15], however, it is assigned to experimental levels above 9 MeV. The band head also comes out close to this energy, while in the DAMD it is overestimated only moderately by 1.3 MeV. It seems that all three models have difficulty reproducing the low band-head energy. Theoretical $B(E2)$ values are available only from the DAMD and the SACM calculations, but there are no experimental data to compare them with. The SACM predicts 3 to 4 times stronger transitions here (see Table V). Nevertheless, it is notable that the trend of the transitions within the band shows rather similar pattern in the two models. There is one experimental $B(E1)$ value for a transition from the 2^- state to the 2^+ band-head state of the 2^+ band. It is relatively strong, which seems to confirm the DAMD and SACM expectations, according to which these two bands have similar structure. SACM calculations on these electric dipole transitions are displayed in Table VI.

In contrast with the 2^- band, the 1^- band is interpreted in the DAMD as a molecular band with moderate $\alpha+^{16}\text{O}$ cluster structure with one of the two valence neutron excited

to a higher orbit. The same band is interpreted as a $1\hbar\omega$ excitation with (11,1) SU(3) character, which corresponds to an elongated, slightly triaxial structure. In the GCM this band consists of states with dominantly $\alpha + {}^{18}\text{O}(2^+)$ character. Both the DAMD and the GCM reproduce the band-head energy of this band, while in the SACM it comes out about 3 MeV too low. Despite the different results on the energy spectrum, the electric quadrupole transitions are rather similar in the three models concerning both the intensity and the trend of transitions within this band (see Table V). The only exception is the $2^- \rightarrow 1^-$ transition, which is stronger in the SACM.

The third negative-parity band is 0_1^- , which is interpreted in the DAMD as a structure with prominent $\alpha + {}^{16}\text{O}$ internal structure. In the SACM the lowest lying 0^- band is expected to be the one with $1\hbar\omega$ excitation and $(\lambda, \mu)\kappa = (9, 2)0$ character. This would be the negative-parity equivalent of the (8,2)0 ground-state band. The band-head energy of this band comes out about 3 MeV too high both in the DAMD and the SACM, while it is only 1.2 MeV higher in the GCM, where the band assignment differs from that of the other models. Despite this result, the electric quadrupole transitions are rather similar for this band in the SACM and the GCM, while the DAMD results are more than a factor of 2 stronger. As it will be discussed in the next subsection, the equivalent of this DAMD band might be the 0_2^- molecular band that appears both in the GCM and the SACM and has electric quadrupole transitions comparable to those obtained in the DAMD for the 0_1^- band. E2 transitions from the 0_1^- band to the 1^- band are available in the GCM and have $B(\text{E}2)$ in the order of a few W.u., except for one transition, which is significantly stronger. In the SACM these transitions are zero if the $q_C = q_R$ choice is made in Eq. (8), but can acquire moderate non-zero values in the general case. Calculations are also available for electric dipole transitions to the ground-state band in the GCM and the SACM. These are in the order of 10^{-3} W.u. in both models, similarly to the transitions from the $K^\pi = 2^-$ band to the 2^+ band. This seems to confirm that these four bands may be associated to similar structure.

It is seen that in contrast with the case of the positive-parity sector, the simple Hamiltonian (6) that sets the relative position of bands via the second-order SU(3) Casimir invariant (essentially the $Q \cdot Q$ interaction) and κ^2 was unable to reproduce the relative position of the 2^- , 0_1^- and 1^- bands, as the first two came out too high, while the last one too low. The order of bands could be restored by a further $(-1)^{n_\pi + \kappa}$ type term, which was used in

several applications of the SACM to *sd*-shell nuclei [19, 22]. However, in those cases the experimental spectrum was much richer (both in energy levels and bands), so we decided to omit this term in the present study in order to keep the number of parameters as low as possible.

There are further negative-parity model states with $1\hbar\omega$ excitation predicted by the SACM, which are not seen in the DAMD and the GCM. These are assigned to the (7,3) and (5,4) SU(3) configuration and correspond to compact triaxial structures, similar to the (6,3) and (4,4) configurations with $0\hbar\omega$ excitation in the positive-parity sector of the spectrum. The lowest bands should start with a 3^- and a 4^- band-head state, and the former (7,3)3 band should be connected to the 2^+ band with E1 transitions of the order 10^{-4} W.u. In Table III we tentatively assigned the (7,3)3 band-head state to the $3^-(7.722)$ level, however more spectroscopic data would be needed for a more justifiable assignment. This also applies to our assignment of the $J^\pi = 4^-$ band-head state of the (5,4)4 SACM band: since there are no 4^- states in the experimental energy spectrum [25], we tentatively chose the $(3)^-$ state at $E_x = 8.376$ MeV (see Table III).

C. Molecular orbital bands

All three models predict both positive- and negative-parity nuclear molecular bands with large deformation and pronounced α -cluster character a few MeV above the $\alpha + {}^{18}\text{O}$ threshold. In the DAMD these bands are obtained from a hybrid-GCM extension by including $\alpha + {}^{18}\text{O}_{\text{g.s.}}$ configuration in the basis [17]. The extended model predicts a 0^+ and a 0^- band starting near 14-15 MeV. In the GCM approach [15] there appears the 0_3^+ band starting at 10.28 MeV and the 0_2^- band starting at 11.47 MeV. The 0_3^+ band has dominantly $\alpha + {}^{18}\text{O}(0^+)$ character for low J , while for increasing J the $\alpha + {}^{18}\text{O}(2^+)$ character increases. This latter structure dominates the 0_2^- band. Similar α -cluster bands are also present in the SACM basis in this energy range. A difference with respect to the DAMD calculations is that the $\alpha + {}^{18}\text{O}$ model space of the SACM also contains configurations with the first excited 2^+ (and 4^+) state of ${}^{18}\text{O}$. Actually, the model states contain a mixture of these states and the ground state of ${}^{18}\text{O}$ in proportions prescribed by the SU(3) symmetry. This mixed character makes them similar to the states obtained in the GCM calculations.

Furthermore, besides the 0^+ and 0^- bands with this structure the SACM also predicts

1^+ , 2^+ , 1^- and 2^- bands with the same $n\hbar\omega$ excitation. These latter bands have a slightly triaxial structure, while the $(n,0)0$ type bands have definite prolate character. Bands with $K \neq 0$ contain also unnatural-parity levels, but the experimental identification of such levels may be difficult. According to Fig. 1 the best candidates for the positive-parity molecular orbital bands are the $2\hbar\omega$ (12,1)1, (10,2)0 and the $4\hbar\omega$ (16,0)0 states of the SACM. The simple Hamiltonian (6) with parameters fitted mainly to the lower-lying levels gives as band-head energy 12.067, 15.803 and 18.758 MeV, respectively. The in-band E2 transitions are rather strong (larger than 25 W.u.). These values are close to those obtained in the GCM for the 0_3^+ band (40 to 50 W.u.) [15]. In the GCM there are also weak E2 transitions from this band to the 0_1^+ ground-state band (0.7 to 2.8 W.u.). In the SU(3) dynamical symmetry approximation of the SACM the corresponding transitions are forbidden from the (12,1)1 and (16,0)0 bands, but they are allowed from the (10,2)0 band. Calculations on the electromagnetic transition data are not available for the 0_3^+ band in the DAMD [17]. The deformation of this band that is characterized by the rotational constant is also close in the DAMD and the GCM, and is in the range obtained for the (12,1)1 and (10,2)0 SACM bands.

There is another positive-parity band in the ETCM [16] expected at $E_x=12.8$ MeV and identified as 0_5^+ . This band is also characterized by strong (~ 45 W.u.) E2 transitions and very weak transitions (< 1 W.u.) to the ground-state band. The rotational constant of this band is similar to that of the 0_3^+ band discussed above, which, however, does not appear in the ETCM calculations.

The 0_2^- negative-parity molecular orbital band is seen in the GCM [15] and the hybrid-GCM extension of the DAMD [17] at 11.47 and 14.8 MeV, respectively. The typical in-band E2 transitions are found rather strong (35 to 40 W.u.) in the GCM, while there is no similar calculation in Ref. [17]. Candidates for this band in the SACM can be those with the SU(3) labels (15,0)0 or (13,1)1 starting at 12.8 and 18.1 MeV, respectively. Transitions in both come out in the range of < 45 W.u. It is notable that in the DAMD similar $B(E2)$ values are obtained for the 0_1^- band, which has the most prominent α -cluster character in the DAMD according to Ref. [17]. It is also suggested that this and the 0_2^+ band are parity doublets. Since in the SACM the latter band is assigned to (14,0)0, a natural interpretation of this finding would be assigning (15,0)0 to the 0_1^- band of the DAMD.

The ETCM [16] also describes a negative-parity band at $E_x = 12.58$ MeV, which is

expected to contain the close-lying pairs of 1^- , 3^- , 7^- and 9^- states found experimentally [28]. However, the calculated in-band electric quadrupole transitions are much weaker (< 15 W.u.) than those found for the molecular orbital bands in the GCM and the SACM. Furthermore, the ETCM predicts relatively strong (10^{-3} W.u.) electric dipole transitions to the ground-state band indicating that they have similar structure. In the SACM these features are similar to those of the (7,3)1 band, which is expected to appear in this energy domain. The splitting of α -cluster states [28] is reproduced only in the ETCM, which associates rather rich structure to the core ^{18}O nucleus.

V. SUMMARY AND CONCLUSIONS

There are several bands established experimentally in the spectrum of ^{22}Ne (e.g. 0_1^+ , 2^+ , 2^-), however, the assignment of levels to further bands is generally ambiguous due to the lack of spectroscopic data. The SACM describes all the well-established bands rather well especially in the positive-parity sector, while the band-head energies are less well reproduced for negative parity. This seems to indicate that the simple five-parameter phenomenological Hamiltonian of the SACM may be a crude approximation, at least for negative-parity bands. It is notable though, that some band-head energies are not reproduced accurately in other models either.

The comparison with the results of microscopic models such as the DAMD [17] and the GCM [15] reveals that there are many similarities with the predictions of these models. The three models describe bands with relatively large deformation both for positive and negative parity and the expected properties of these bands (0_1^+ , 2^+ , 0_2^+ , 1^- , 0_2^-) generally coincide. The 1^+ band is seen only in the SACM and the GCM but not in the DAMD, which may indicate that the corresponding energy surface might not be identified in the latter model due to the small deformation. It is notable that the results of the three cluster models on low-lying positive-parity states agree rather well with shell model calculations [27] assuming an $(sd)^6$ configuration and an inert ^{16}O core. In the case of the SACM this may be explained by the fact that the SACM model space with $0\hbar\omega$ excitation is a subset of the harmonic oscillator shell model.

The 0_2^+ band has well-developed α -cluster structure with large deformation in the SACM and the DAMD, while these features are less pronounced in the GCM. In this latter model

the 0_3^+ band has marked α -cluster structure, together with the 0_2^- band. Such molecular bands appear both in the SACM and the DAMD, although in the latter case a hybrid $\alpha + {}^{18}\text{O}_{\text{g.s.}}$ extension of the model is necessary.

The internal excitation of the ${}^{18}\text{O}$ cluster plays an important role both in the GCM and the SACM. In the GCM several bands are interpreted as structures built on the 2_1^+ level of ${}^{18}\text{O}$, while this configuration and that with the 4_1^+ state appear in the SACM states due to the assumed SU(3) symmetry. There are relatively numerous calculated values on electric quadrupole and dipole transitions in the GCM, which allows a straightforward comparison of the two models. The selection rules of these transitions are rather similar in the two models in the sense that transitions forbidden due to the assumed SU(3) dynamical symmetry in the SACM correspond to rather weak transitions in the GCM. These results indicate that the 0_1^+ , 2^+ and 2^- bands, as well as the 0_1^- band present in both models may have similar structure. This feature is also confirmed by the DAMD calculations with the exception that the 0_1^- band there has more pronounced deformation and α -cluster structure. It is possible that this DAMD band should correspond to the 0_2^- band of the GCM and the (15,0) SU(3) band in the SACM.

The experimental confirmation of the predictions given by the three models is missing in most cases, especially concerning electric quadrupole and dipole transitions. Such spectroscopic information would also make it possible to put the tentative band assignments on a more firm basis.

The similarities between the band structure and the properties of bands described simultaneously in the SACM and GCM have already been noticed in earlier calculations on α -cluster states of other nuclei, such as ${}^{18}\text{O}$ [18]. It is probable that this similarity originates from the fact that the GCM employs an harmonic oscillator basis with a common oscillator constant for each cluster. The SU(3) dynamical symmetry of the SACM is also based on this harmonic oscillator assumption. The fully microscopic model space of this model contains SU(3) shell model basis constructed from antisymmetrized harmonic oscillator states. This common background may be manifested in similar matrix elements and selection rules despite the different construction of the operators.

A systematic study of core+ α states of nuclei in the ${}^{20}\text{Ne}$ to ${}^{24}\text{Mg}$ region seems worthwhile. A similar study has already been performed in the region between the ${}^{16}\text{O}$ to ${}^{20}\text{Ne}$ nuclei and it was found that the SACM parameters vary smoothly in this domain [20].

Acknowledgments

This work was supported by the OTKA (grant no. K72357) and the JSPS–MTA Japanese–Hungarian cooperation. The author is indebted to M. Kimura for valuable discussions.

-
- [1] Y. Fujiwara, H. Horiuchi, K. Ikeda, M. Kamimura, K. Katō, Y. Suzuki, and E. Uegaki, *Prog. Theor. Phys. Suppl.* **68**, 60 (1980);
P. Descouvemont and D. Baye, *Phys. Rev. C* **31**, 2274 (1985).
 - [2] B. Buck, H. Friedrich, and A. A. Pilt, *Nucl. Phys. A* **290**, 204 (1977).
 - [3] S. Saito, *Prog. Theor. Phys.* **40**, 893 (1968);
41, 705 (1969).
 - [4] J. Cseh, *Phys. Lett. B* **281**, 173 (1992);
J. Cseh and G. Lévai, *Ann. Phys. (N.Y.)* **230**, 165 (1994).
 - [5] J. P. Elliott, *Proc. Roy. Soc. A* **245**, 128 (1958);
245, 562 (1958).
 - [6] M. Harvey, *Advances in Nuclear Physics* **1**, 67 (1968).
 - [7] K. Wildermuth and Th. Kanellopoulos, *Nucl. Phys.* **7**, 150 (1958).
 - [8] B. F. Bayman and A. Bohr, *Nucl. Phys.* **9**, 596 (1958/59).
 - [9] J. Cseh, A. Algora, J. Darai, and P. O. Hess, *Phys. Rev. C* **70**, 034311 (2004);
J. Cseh, J. Darai, W. Sciani, Y. Otani, A. Lépine-Szily, E. A. Benjamim, L. C. Chamon, and R. Lichtenthaler, *Phys. Rev. C* **80**, 034320 (2009);
J. Darai, J. Cseh, N. V. Antonenko, G. Royer, A. Algora, P. O. Hess, R. V. Jolos, and W. Scheid, *Phys. Rev. C* **84**, 024302 (2011);
J. Darai, J. Cseh, and D. G. Jenkins, *Phys. Rev. C* **86**, 064309 (2012).
 - [10] P. O. Hess and G. Lévai, *Int. J. Mod. Phys. E* **14**, (2005) 845;
G. Lévai and P. O. Hess, *Eur. Phys. J. A direct (e) Suppl.* **27**, (2006) 277.
 - [11] W. von Oertzen, *Z. Phys. A* **354**, 37 (1996);
N. Itagaki and S. Okabe, *Phys. Rev. C* **61**, 044306 (2000);
P. Descouvemont, *Nucl. Phys. A* **699**, 463 (2002);

- W. von Oertzen, M. Freer, and Y. Kanada-En'yo, Phys. Rep. **424**, 175 (2006).
- [12] W. von Oertzen, Eur. Phys. J. A **11**, 403 (2001).
- [13] Y. Kanada-En'yo, H. Horiuchi, and A. Ono, Phys. Rev. C **52**, 628 (1995);
A. Dote, H. Horiuchi, and Y. Kanada-En'yo, Phys. Rev. C **56**, 1844 (1997);
Y. Kanada-En'yo and H. Horiuchi, Phys. Rev. C **68**, 014319 (2003).
- [14] M. Kimura, Phys. Rev. C **69**, 044319 (2004).
- [15] P. Descouvemont, Phys. Rev. C **38**, 2397 (1988).
- [16] M. Dufour and P. Descouvemont, Nucl. Phys. A **726**, 53 (2003).
- [17] M. Kimura, Phys. Rev. C **75**, 034312 (2007).
- [18] G. Lévai, J. Cseh, and W. Scheid, Phys. Rev. C **46**, 548 (1992).
- [19] K. Varga and J. Cseh, Phys. Rev. C **48**, 602 (1993);
Zs. Fülöp, G. Lévai, E. Somorjai, Á. Z. Kiss, J. Cseh, P. Tikkanen, and J. Keinonen, Nucl. Phys. A **604**, 286 (1996);
G. Lévai, J. Cseh and P. Van Isacker, Eur. Phys. J. A **12**, 305 (2001);
L. H. de la Peña, P. O. Hess, G. Lévai, and A. Algora, J. Phys G **27**, 2019 (2001).
- [20] G. Lévai and J. Cseh, Phys. Lett. B **381**, 1 (1996).
- [21] G. Lévai, J. Cseh, and P. Van Isacker, J. Phys. G **34**, 1729 (2007).
- [22] J. Cseh, G. Lévai, and W. Scheid, Phys. Rev. C **48**, 1724 (1993);
J. Cseh, R. K. Gupta, and W. Scheid, Phys. Lett. B **299**, 205 (1993);
J. Cseh, Phys. Rev. C **50**, 2240 (1994);
J. Cseh, G. Lévai, A. Ventura, and L. Zuffi, Phys. Rev. C **58**, 2144 (1998);
J. Cseh, G. Lévai, P. O. Hess, and W. Scheid, Few-Body Syst. **29**, 61 (2000).
- [23] H. Yépez-Martínez, M. J. Ermanotov, P. R. Fraser, and P. O. Hess, Phys. Rev. C **86**, 034309 (2012).
- [24] H. A. Naqvi and J. P. Draayer, Nucl. Phys. A **516**, 351 (1990).
- [25] <http://www.nndc.bnl.gov/databases/databases.html>
- [26] P. Raghavan, Atom. Data Nucl. Data Tabl. **42**, 189 (1989).
- [27] B. M. Freedom and B. H. Wildenthal, Phys. Rev. C **6**, 1633 (1972).
- [28] G. V. Rogachev et al., Phys. Rev. C **64** (2001) 051302.

TABLE II: Assignment of positive-parity experimental ^{22}Ne states to the SACM states. $E_{\text{Th.}}$ is the result of a simple fit described in Subsection III B. States with $J \leq 8$ are displayed. For bands expected to lie higher only the lowest member of the band is indicated.

$n_\pi(\lambda, \mu)\kappa$	J^π	$E_{\text{Th.}}$	K^π	$J^\pi(E)_{\text{Exp.}}$
		(MeV)		(MeV)
8(8,2)0	0^+	0	0_1^+	$0^+(0)$
	2^+	0.865		$2^+(1.275)$
	4^+	2.882		$4^+(3.358)$
	6^+	6.053		$(6^+)(6.310)$
	8^+	10.377		$(8^+)(11.032)$
8(8,2)2	2^+	4.349	2^+	$2^+(4.456)$
	3^+	5.214		$3^+(5.641)$
	4^+	6.367		$(4)^+(5.524)$
	5^+	7.808		$(5^+)(7.422)$
	6^+	9.538		
8(6,3)1	1^+	4.404	1^+	$1^+(5.332)$
	2^+	5.129		$2^+(5.363)$
	3^+	6.217		$3^+(6.635)$
	4^+	7.668		$4^+(6.347)$
	5^+	9.481		
8(6,3)3	3^+	14.985		
8(4,4)0	0^+	5.154		$0^+(7.341)$
	2^+	6.503		
	4^+	9.651		
8(4,4)2	2^+	11.940		
8(4,4)4	4^+	31.936		
10(14,0)0	0^+	6.230	0_2^+	$0^+(6.234)$
	2^+	6.650		$2^+(7.665)$
	4^+	7.630		$(4)^+(8.076)$
	6^+	9.169		
	8^+	11.268		
10(12,1)1	1^+	12.967		
10(10,2)0	0^+	15.803		

TABLE III: The same as Table II for negative-parity states of ^{22}Ne . States with $J \leq 7$ are displayed.

$n_\pi(\lambda, \mu)\kappa$	J^π	$E_{\text{Th.}}$	K^π	$J^\pi(E)_{\text{Exp.}}$
		(MeV)		(MeV)
9(11,1)1	1^-	3.938	1^-	$1^-(7.051)$
	2^-	4.330		$2^-(7.665)$
	3^-	4.918		$(3)^-(8.376)$
	4^-	5.702		
	5^-	6.682		
9(9,2)0	1^-	8.370	0_1^-	$1^-(6.691)$
	3^-	9.583		$3^-(7.406)$
	5^-	11.766		
	7^-	14.920		
9(9,2)2	2^-	7.194	2^-	$2^-(5.146)$
	3^-	7.922		$3^-(5.910)$
	4^-	8.892		
	5^-	10.105		
9(7,3)1	1^-	11.226		
9(7,3)3	3^-	8.609		$3^-(7.722)$
9(5,4)0	1^-	14.388		
9(5,4)2	2^-	12.593		
9(5,4)4	4^-	7.567		$(3)^-(8.376)$
11(15,0)0	1^-	12.843	0_2^-	$1^-(12)$
	3^-	13.461		
	5^-	14.572		
	7^-	16.178		
11(13,1)1	1^-	18.137		

TABLE IV: $B(E2)$ values in W.u. for transitions between states assigned to the same (λ, μ) representations. To fit the $q_R = q_C$ parameters the transition marked with asterix was used. Experimental data are from Ref. [25].

$[n_\pi(\lambda, \mu)\kappa]_i$	J_i^π	$[n_\pi(\lambda, \mu)\kappa]_f$	J_f^π	$B_{\text{Exp.}}(E2)$	$B_{\text{Th.}}(E2)$	DAMD [17]	GCM [15]
8(8,2)0	2 ⁺	8(8,2)0	0 ⁺	12.5±0.5	13.38	14.9	8.4
	4 ⁺		2 ⁺	17.5±0.4	17.50*	20.5	9.5
	6 ⁺		4 ⁺	13.7±1.7	16.06	15.8	10.2
	8 ⁺		6 ⁺		12.11	10.8	7.9
8(8,2)2	3 ⁺	8(8,2)2	2 ⁺		23.88	15.5	18.5
	4 ⁺		2 ⁺		7.09	5.4	4.9
	4 ⁺		3 ⁺		17.11	8.4	
	5 ⁺		3 ⁺		10.59	7.4	
	5 ⁺		4 ⁺		12.55	11.4	6.4
8(8,2)2	2 ⁺	8(8,2)0	0 ⁺	> 0.26	0.67		0.055
	2 ⁺		2 ⁺	> 0.21	1.28		0.30
	2 ⁺		4 ⁺		0.13		
	3 ⁺		2 ⁺		1.20		0.16
	3 ⁺		4 ⁺		0.97		
	4 ⁺		2 ⁺	0.093 ± 0.023	0.27		0.70
	4 ⁺		4 ⁺		1.58		
	4 ⁺		6 ⁺		0.44		
	4 ⁺		4 ⁺		0.13		
8(6,3)1	2 ⁺	8(6,3)1	1 ⁺		8.87		
	3 ⁺		1 ⁺		10.05		
	3 ⁺		2 ⁺		12.31		
	4 ⁺		2 ⁺		7.80		
	4 ⁺		3 ⁺		1.00		
	5 ⁺		3 ⁺		11.65		
	5 ⁺		4 ⁺		6.11		
8(4,4)0	2 ⁺	8(4,4)0	0 ⁺		6.97		
	4 ⁺		2 ⁺		8.80		
10(14,0)0	2 ⁺	10(14,0)0	0 ⁺	30	29.32	29.0	5.9
	4 ⁺		2 ⁺		40.13	32.1	7.1

TABLE V: $B(\text{E}2)$ values calculated for negative-parity levels.

$[n_\pi(\lambda, \mu)\kappa]_i$	J_i^π	$[n_\pi(\lambda, \mu)\kappa]_f$	J_f^π	$B_{\text{Th.}}(\text{E}2)$	DAMD [17]	GCM [15]
9(11,1)1	2 ⁻	9(11,1)1	1 ⁻	36.04	11.4	15.5
	3 ⁻		1 ⁻	15.84	13.4	17.5
	3 ⁻		2 ⁻	11.44	12.9	17.2
	4 ⁻		2 ⁻	24.94	12.1	22.2
	4 ⁻		3 ⁻	11.35	16.8	
	5 ⁻		3 ⁻	22.85		
	5 ⁻		3 ⁻	3.50		
9(9,2)0	3 ⁻	9(9,2)0	1 ⁻	20.08	41.4	20.6
	5 ⁻		3 ⁻	21.25	47.1	27.5
	7 ⁻		5 ⁻	18.64	46.8	17.2
	9 ⁻		7 ⁻	13.77	43.9	
9(9,2)2	3 ⁻	9(9,2)2	2 ⁻	28.45	6.5	
	4 ⁻		2 ⁻	8.80	2.1	
	4 ⁻		3 ⁻	21.27	4.5	
	5 ⁻		3 ⁻	12.92	4.1	
	5 ⁻		4 ⁻	13.35	5.1	
9(9,2)0	1 ⁻	9(9,2)2	3 ⁻	0.94		
	3 ⁻		2 ⁻	1.28		
	3 ⁻		3 ⁻	0.41		
	3 ⁻		4 ⁻	1.32		
	3 ⁻		5 ⁻	0.332		
9(7,3)1	2 ⁻	9(7,3)1	1 ⁻	26.43		
	3 ⁻		1 ⁻	8.00		
	3 ⁻		2 ⁻	4.04		
	4 ⁻		2 ⁻	16.18		
	4 ⁻		3 ⁻	9.65		
11(15,0)0	3 ⁻	11(15,0)0	1 ⁻	42.14		38.8
	5 ⁻		3 ⁻	47.04		36.5
	7 ⁻		5 ⁻ $\bar{3}_1$	45.78		
	9 ⁻		7 ⁻	41.20		

TABLE VI: $B(\text{E1})$ values in 10^{-3} W.u. for transitions between states belonging to the $(\lambda, \mu) = (9, 2)$ and $(8, 2)$ representations. To fit the d_R parameter the transition marked with asterix was used. The experimental value for this transition is $1.5 \pm 0.4 \cdot 10^{-3}$ W.u. [25].

$[n_\pi(\lambda, \mu)\kappa]_i$	J_i^π	$[n_\pi(\lambda, \mu)\kappa]_f$	J_f^π	$B_{\text{Th.}}(\text{E1})$	GCM [15]
9(9,2)0	1^-	8(8,2)0	0^+	0.83	0.0024
			2^+	1.23	0.49
			2^+	1.24	3.2
			4^+	0.82	0.91
9(9,2)2	2^-	8(8,2)2	2^+	1.5*	
			3^+	0.56	
			2^+	0.70	
			3^+	0.73	
			4^+	0.62	